



PCCP

Semiconductor-metal transition induced by nanoscale stabilization

Journal:	<i>Physical Chemistry Chemical Physics</i>
Manuscript ID:	CP-COM-12-2014-005619.R1
Article Type:	Communication
Date Submitted by the Author:	08-Jan-2015
Complete List of Authors:	Hörmann, Nicolas; Universität Ulm, Gross, Axel; Universität Ulm, Abteilung Theoretische Chemie Kaghazchi, Payam; Universität Ulm, Institut für Elektrochemie

SCHOLARONE™
Manuscripts

Semiconductor-metal transition induced by nanoscale stabilization

Nicolas G. Hörmann and Axel Gross

*Helmholtz Institute Ulm (HIU) Electrochemical Energy Storage, Albert-Einstein-Allee 11, 89069 Ulm and
Universität Ulm, Institut für Theoretische Chemie, Albert-Einstein-Allee 11, 89069 Ulm*

Payam Kaghazchi*

Institut für Chemie und Biochemie, Freie Universität Berlin, Takustr. 3, 14195 Berlin, Germany

(Dated: January 7, 2015)

The structure of tin (Sn) nanoparticles as function of size and temperature has been studied using density functional theory and thermodynamic considerations. It is known that bulk Sn undergoes a transition from the semiconducting α -phase to the metallic β -phase at temperatures higher than 13.2°C under atmospheric pressure. Here we show that, independent of temperature, Sn nanoparticles smaller than 8 nm diameter always crystallize in the β phase structure in thermodynamic equilibrium, and up to a size of 40 nm of the Sn nanoparticles this metallic phase is stable at all reasonable ambient temperatures ($\gtrsim -40$ °C). The transition to the metallic phase is caused by nanoscale stabilization due to the lower surface energies of the β phase. This study suggests that the atomic structure and conductivity of nanostructured Sn anodes can change dramatically with size and temperature. This finding has implication for understanding the performance of future Li-based batteries since Sn nanostructures are considered as one of the most promising anode materials, but the mechanism of nanoscale stabilization might be used as a design strategy for other materials.

PACS numbers:

Keywords:

I. INTRODUCTION

Tin (Sn) has been used for many years in electronics devices and metal food containers. Sn has also potential applications in the field of optoelectronics¹⁻³ and topological insulators⁴⁻⁸. In particular, Sn is a very promising anode material for future Li-based batteries due to a high theoretical storage capacity of ~ 990 mAh/g which is 2.5 times larger than that of currently-used graphitic carbon⁹. Recent studies have, however, shown that only nanostructured Sn electrodes can provide large capacities (near the theoretical value) and long cycle lives^{10,11}. This requires a stabilization of Sn nanostructures against structural damages and crack formation during lithiation/delithiation⁹⁻¹⁵. Moreover, Sn is superior to carbon for Na-based^{16,17} and F-based batteries¹⁸.

Experiments indicate that under atmospheric pressure, at temperatures lower than 13.2°C bulk Sn has a diamond structure (α -phase), while at higher temperatures it has a tetragonal structure (β -phase)¹⁹. The $\alpha \rightarrow \beta$ phase transition is accompanied by a dramatic reduction of volume and transition from semiconductor to metal.

In this work, using DFT calculations in conjunction with thermodynamic considerations we study the electronic and atomic structures as well as stability of bulk, surfaces, and nanoparticles of α -Sn and β -Sn. We show that a semiconductor-metal transition can be induced by controlling the size of Sn nanoparticles. As β -Sn has much lower surface energies than α -Sn, small β -Sn nanoparticles become thermodynamically stabilized at environmental conditions at which α -Sn is stable as a bulk material. This also induces a transition from the semiconducting state of α -Sn to the metallic state of β -

Sn. Nanoscale stabilization has also been predicted for sodium oxide²⁰, but in this material it is not accompanied by a semiconductor-metal transition. We propose that the nanoscale stabilization of Sn nanocrystallites addressed in this work can be a key factor in controlling the performance of Li batteries with Sn as an anode material, as the α - β phase transition is expected to decrease lifetimes and cyclability. The mechanism of nanoscale stabilization, however, might well also be operative in other materials.

II. METHODS

We calculate the surface energies (γ_i) by periodic density functional theory (DFT) calculations within the slab approach by

$$\gamma \approx \frac{E_{\text{slab}}^{\text{tot}} - N_{\text{Sn}} E_{\text{bulk}}^{\text{tot}}}{2A}, \quad (1)$$

where $E_{\text{slab}}^{\text{tot}}$, A , and N_{Sn} are total energy, the surface area, and the number of Sn atoms in the slab, while $E_{\text{bulk}}^{\text{tot}}$ is the total energy of bulk Sn per atom.

We determine the equilibrium shape of Sn nanoparticles by using Wulff's theorem²¹. To study the $\alpha \leftrightarrow \beta$ phase transition in Sn nanoparticles as function of size we calculate the Gibbs free energies per atom for nanoparticles (G_{tot}/N). We assume G_{tot}/N of a given particle shape to be equivalent to that of a spherical particle of the same number of atoms (N) or volume (V) at a fixed density (ρ). The relation between energetics of a polyhedral particle and its equivalent spherical particle is given in Tab. I.

TABLE I: Bulk and surface energetics a particle of arbitrary shape and a spherical particle.

property	arbitrary particle	spherical particle
Bulk energy	$G_{\text{bulk}} = g_{\text{bulk}} \cdot N = g_{\text{bulk}} \cdot V \rho$	$G_{\text{bulk}} = g_{\text{bulk}} \cdot \frac{4}{3} \pi r^3 \rho$
Surface energy	$G_{\text{surf}} = \sum_i A_i \gamma_i$	$G_{\text{surf}} = 4\pi r^2 \bar{\gamma}$

The equivalence of bulk energies as well as surface energies result in:

$$r = \left(\frac{N}{\frac{4}{3}\pi\rho} \right)^{\frac{1}{3}} = \left(\frac{V}{\frac{4}{3}\pi} \right)^{\frac{1}{3}} \quad (2)$$

$$\bar{\gamma} = \frac{\sum_i \gamma_i A_i}{4\pi \left(\frac{V}{\frac{4}{3}\pi} \right)^{\frac{2}{3}}}, \quad (3)$$

where $\bar{\gamma}$ is the mean surface energy for a Wulff-shaped nanoparticle or the surface energy of its equivalent spherical particle. r is the radius of the sphere.

The total Gibbs free energy per atom is then given by:

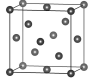
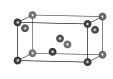
$$\begin{aligned} \frac{G_{\text{tot}}}{N} &= \frac{G_{\text{bulk}} + G_{\text{surf}}}{N} = \frac{G_{\text{bulk}}}{N} + \frac{4\pi\bar{\gamma}r^2}{\frac{4}{3}\pi\rho r^3} = \quad (4) \\ &= \frac{G_{\text{bulk}}}{N} + \bar{\gamma} \frac{3}{\rho r} \stackrel{\text{eq. 2}}{=} \frac{G_{\text{bulk}}}{N} + \bar{\gamma} \sqrt[3]{\left(\frac{6}{\rho}\right)^2 \frac{\pi}{N}}, \end{aligned}$$

where G_{bulk} is the Gibbs free energy of bulk Sn.

The phase transition of Sn is caused by the temperature dependence of the free energy of the lattice vibrations²². In order to determine the temperature-dependent phase transition for a Sn nanoparticle of a given size we determine the Gibbs free energy of bulk Sn by

$$G_{\text{bulk}} \approx U + F_{\text{vib}}, \quad pV \approx 0, \quad (5)$$

TABLE II: The atomic structures, lattice constants, volume per unitcell, and cohesive energies of α -Sn and β -Sn polymorphs calculated with GGA-PBE. The corresponding experimental (shown by exp.) and previous GGA-PBE (in parentheses) values are also given.

	α -Sn	β -Sn
		
a (Å)	6.654 (6.64 ^c) exp.: 6.480 ^a	5.967 (5.96 ^c) exp.: 5.831 ^b
b (Å)	6.654	5.967
c (Å)	6.654	3.185 exp.: 3.181 ^b
V/atom (Å ³)	36.83	28.35
E_{coh} (eV)	3.202 (3.19 ^c) exp.: 3.12 ^d	3.165 (3.13 ^c) -

^a ref.³¹, ^b ref.³², ^c ref.³⁰, ^d ref.³³

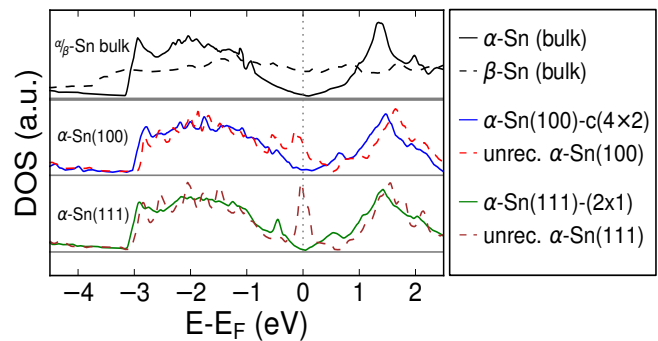


FIG. 1: Density of states (DOS) of α and β -Sn structures near the Fermi level (shifted to 0 eV).

where U is the total inner energy of the nanoparticle comprising a bulk contribution proportional to volume.

We estimate F_{vib} using a simple Debye model expression

$$\begin{aligned} \frac{F_{\text{vib}}}{N} &= 3k_B T_D \left[\frac{3}{8} + \theta \ln(1 - e^{-1/\theta}) \right. \\ &\quad \left. - \theta^4 \int_0^{\frac{1}{\theta}} \frac{x^3}{e^x - 1} dx \right], \quad \theta = \frac{T}{T_D}, \quad (6) \end{aligned}$$

where T_D is the Debye temperature. The first term corresponds to zero-point vibrations and the rest are a combination of entropy and energy terms. We use experimental values of $T_D(\alpha\text{-Sn}) = 260$ K and $T_D(\beta\text{-Sn}) = 170$ K²³, which give similar free energy trends to *ab initio* phonon calculations²². Since the zero-point energy is described by the first term of eq. 6, we replace U_{bulk} by $E_{\text{bulk}}^{\text{tot}}$ in eq. 5, where $E_{\text{bulk}}^{\text{tot}}$ is the ground state energy of the given polymorph.

Total energy calculations have been performed using the Vienna Ab initio Simulation Package (VASP)^{24,25} within the generalized gradient approximation (GGA) of Perdew-Burke-Enzerhof (PBE)²⁶. As spin-orbit has a minor influence on the energetics of Sn²⁷, we consider only scalar relativistic effects, which are included in the PAW pseudopotentials^{28,29}. Computational parameters were chosen to obtain an accuracy of ~ 1 meV/atom and ~ 0.5 meV/Å² in surface energy (plane wave cutoff: 220 eV, k -point meshes: $6 \times 6 \times 6$ (α -Sn), $9 \times 9 \times 15$ (β -Sn)).

III. RESULTS AND DISCUSSIONS

The structures of α -Sn and β -Sn as well as their lattice constants and cohesive energies are listed in Tab. II. The values are in fair agreement with experiment and previous DFT-PBE calculations³⁰. Metallic and insulating properties of bulk β -Sn and α -Sn, respectively (see Fig. 1), as well as higher stability of the latter at 0 K are correctly reproduced.

Using the theoretical lattice constants, we model all

TABLE III: Surface free energies of different α -Sn surfaces and their contributions to the total surface area of α -Sn nanoparticles.

		α -Sn surfaces									
		{100}	{100}	{100}	{111}	{111}	{111}	{211}	{221}	{210}	{110}
		<i>unrec.</i>	<i>pert.</i>	$c(4 \times 2)$	<i>unrec.</i>	<i>pert.</i>	(2×1)	<i>pert.</i>	<i>pert.</i>		
γ (meV/Å ²)		55.5	32.2	30.3	42.0	36.8	33.2	35.3	35.4	35.9	36.0
contribution (%)		-	-	45.8	-	-	27.2	6.2	9.9	3.4	7.5

TABLE IV: Surface free energies of different β -Sn surfaces and their contributions to the total surface area of β -Sn nanoparticles.

		β -Sn surfaces										
		{100}	{101}	{201}	{122}	{112}	{012}	{110}	{001}	{111}	{211}	{221}
γ (meV/Å ²)		23.6	25.3	25.5	26.4	26.5	26.7	26.9	27.8	28.1	29.2	30.3
contribution (%)		29.4	15.8	24.6	10.5	1.1	1.2	15.0	-	0.5	1.6	0.4

possible low-index surfaces as well as several high-index surfaces of α and β -Sn (see Tabs III and IV).

As initial surface structures are created from bulk, bulk-truncated structure have highly symmetric atomic configurations and may correspond to local minima of the energy landscape. In order to facilitate the escape from local minima, we perturbed the positions of the surface atoms by changing their coordinates by random vectors with lengths of ≤ 0.3 Å and relaxed the structures. In some cases, cleaving the α -Sn or β -Sn crystal along a particular direction creates two different surface structures depending on which kind of Sn atoms are exposed. Here we report only the most stable ones. For some of the α - and β -Sn surfaces, we find that the resulting perturbed structures (labeled by *pert.*) are energetically more favorable than the corresponding unreconstructed ones (labeled by *unrec.*).

For α -Sn(100) and (111) surfaces (see Fig. 2), besides unreconstructed and randomly perturbed structures, we consider reconstructed structures that have been reported for Si surfaces^{34–36}. The most stable α -Sn surfaces are found to be the reconstructed (100)- $c(4 \times 2)$ and reconstructed (111)- (2×1) surfaces just as in the case of Si with surface energies of 30.3 and 33.2 meV/Å², respectively (Fig. 2 c, f). The (100)- $c(4 \times 2)$ surface,

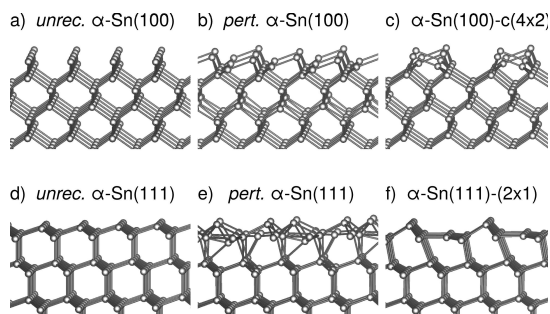


FIG. 2: Structures of different terminations of (100) and (111) α -Sn surfaces. The labels are as described in the text. *unrec.* indicates unreconstructed terminations. *pert.* indicates relaxed structures obtained from randomly perturbed initial structures. $c(4 \times 2)$ and (2×1) indicate the reconstructed structures.

which has a buckled-dimer structure, has a considerably lower surface free energy than the unreconstructed surface (30.3 *vs.* 55.5 meV/Å²). Interestingly, the perturbed structure (see Fig. 2 b) with a surface free energy of 32.2 meV/Å² is only slightly less stable than reconstructed (100)- $c(4 \times 2)$. This is because, similar to the case of the $c(4 \times 2)$ surface, dangling bonds of the perturbed surface are reduced. The surface atoms tend to rebond and lower the bonding states by symmetry-breaking-induced effects such as buckling. Furthermore the reconstruction is able to remove surface metallization of the unreconstructed (100) and (111) surfaces (see Fig. 1).

We also find that the low-index (110) surface as well as high-index (211), (221), and (210) surfaces are only slightly less favorable ($35.3 \text{ meV/Å}^2 \leq \gamma \leq 36 \text{ meV/Å}^2$) than the low-index (100) and (111) surfaces.

The calculated surface energies for β phase have been listed in Tab. IV. The most stable (100) and (101) surfaces are presented in Fig. 3. We find that the average surface free energy of β -Sn is ~ 7.5 meV/Å² lower than that of α -Sn. Similar to the α -Sn phase, low-index (100) is the most favorable surface of the β -Sn phase. The surface free energy of β -Sn(100) is 23.6 meV/Å², which is ~ 7 meV/Å² more stable than α -Sn(100). The high-index vicinal β -Sn(201) surface is only 1.9 meV/Å² less sta-

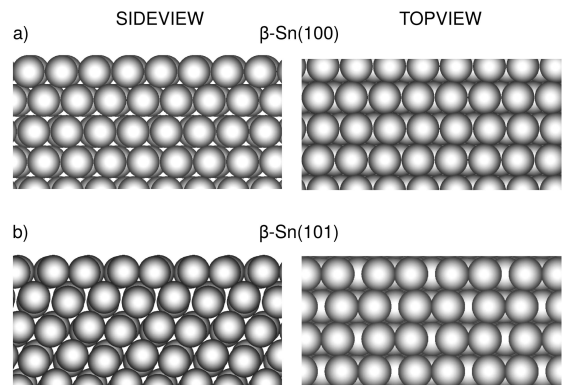


FIG. 3: Side and top views of a) (100) and b) (101) β -Sn relaxed surface structure.

ble than β -Sn(100). In fact the high-index vicinal (122), (112), and (012), are found to be more stable than the low-index β -Sn(001) surface, which is due to the fact that β -Sn(001) is atomically rather open.

Using the calculated surface free energies we construct the equilibrium shapes of α - and β -Sn nanoparticles (Fig. 4). The Wulff shape of α -Sn is cubo-octahedral, dominated by the reconstructed low index $\{100\}$ (blue) and $\{111\}$ (green) facets, which comprise 73% of the total surface area (see table III). The Wulff shape of β -Sn is cubic-like dominated by the $\{100\}$ (blue), $\{101\}$ (green), and $\{201\}$ (white) facets. These surfaces comprise 70% of the total surface area. The partial contribution of high-index vicinal $\{122\}$ surfaces is also $\sim 10\%$ (see table IV). The (201) and (122) surfaces can be viewed as stepped surfaces with plateaus of (100) and (101) termination. Therefore, the β -Sn nanoparticles consist of not only close-packed surfaces but also vicinal surfaces. This is different from what has been observed in the other clean metal nanoparticles such as Rh, Pd, Cu, Ru, Re, and Pt^{37–41} where only only close-packed low-index surface are present in the Wulff shape. This is due to the fact that the coordination loss of surface atoms on low-index surfaces of close-packed bulk structures of aforementioned metals is often small. We attribute the different behavior of β -Sn to the relatively low packing density of its bulk, which can lead to a large number of coordination loss of surface atoms on its low-index surfaces (*e.g.* β -Sn(001)).

To study the temperature and size dependent phase transition of bulk Sn, we combine eqs. 3–6. The effective surface energies ($\bar{\gamma}$) in eq. 3 are determined (based on the Wulff-shapes) to be $34.1 \text{ meV}/\text{\AA}^2$ for α -Sn and $27.0 \text{ meV}/\text{\AA}^2$ for β -Sn. For the bulk case ($N_{\text{Sn}} = \infty$), our calculations give a phase transition temperature of $\sim 330 \text{ K}$, which is slightly larger than the experimental value of 286 K . Therefore, it is expected that the phase diagram can qualitatively (within 40 K) describe the phase transition in Sn nanoparticles. Figure 5 shows the phase transition in Sn nanoparticles as function of T and r (and N). The number of Sn atoms N_{Sn} in the range $[2000, \infty[$ were mapped onto $[0, 1]$ via

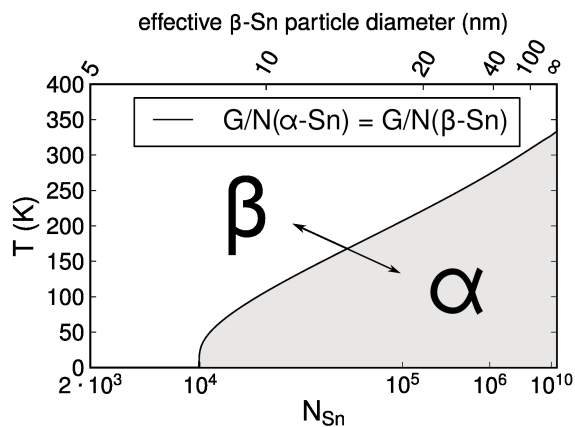


FIG. 5: Temperature-size phase diagram of α - and β -Sn nanoparticles.

$$N_{\text{Sn}} \rightarrow \left(1 - \left[\frac{\log(2000)}{\log(N_{\text{Sn}})}\right]^5\right)^3.$$

The phase diagram shows that β -Sn nanoparticles smaller than 40 nm are stabilized considerably by their smaller surface energy. We predict that those particles should not undergo a transition to the α phase above $\sim -40 \text{ }^\circ\text{C}$, which is relevant for technological applications. Moreover, we find that, independent of temperature, nanoparticles smaller than $\sim 8 \text{ nm}$ (~ 10000 atoms) are stable only in the β -phase.

IV. CONCLUSIONS

In summary, we studied structures and stabilities of surfaces and nanoparticles of α - and β -Sn using DFT calculations together with thermodynamic considerations. For both phases, we found that the low-index (100) surfaces are the most stable surfaces. Generally, β -Sn surfaces are more stable than α -Sn ones. The calculated equilibrium crystal shapes of Sn show that although α -Sn nanoparticles consist mainly of low-index faces, β -Sn nanoparticles are enclosed by not only low-index surfaces but also high-index vicinal surfaces. The lower surface energies of β -Sn lead to a nanoscale stabilization of this metallic phase. Consequently the size of Sn nanoparticles is a tuning knob to increase the temperature window of metallic behavior and avoid the so-called tin pest. Our calculations suggest that Sn nanoparticles smaller than 40 nm should be stable in the metallic β -Sn form down to temperatures of $-40 \text{ }^\circ\text{C}$. This is in particular important in nanostructured Sn anodes of Li-based batteries, as the α - β phase transition is expected to decrease lifetime, cyclability, and electrical conductivity due to the related drastic volume changes^{42,43}. Additional tuning may be obtained by a tailored modifications of surface energies through appropriate surfactants.

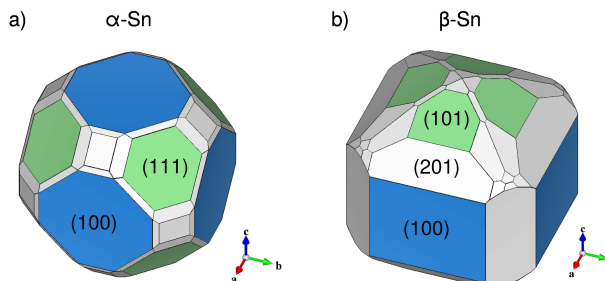


FIG. 4: Equilibrium shapes of clean α - and β -Sn nanoparticles.

V. ACKNOWLEDGMENTS

Computer time was provided by the BW-Grid of the federal state of Baden-Württemberg. Discussions with J.

Rohrer and U. Kaiser are gratefully acknowledged. P. K. gratefully acknowledges support from the “Bundesministerium für Bildung und Forschung“ (BMBF).

-
- * payam.kaghazchi@fu-berlin.de
- ¹ Ng, M.-F. & Tan, T. L. *Nano Lett.* **13**, 4951–4956 (2013).
 - ² Küfner, S., Furthmüller, J., Matthes, L., Fitzner, M. & Bechstedt, F. *Phys. Rev. B* **87**, 235307 (2013).
 - ³ Küfner, S., Furthmüller, J., Matthes, L. & Bechstedt, F. *Nanotechnology* **24**, 405702 (2013).
 - ⁴ Fu, L. & Kane, C. L. *Phys. Rev. B* **76**, 045302 (2007).
 - ⁵ Zhang, F., Kane, C. L. & Mele, E. J. *Phys. Rev. B* **86**, 081303 (2012).
 - ⁶ Zhang, F., Kane, C. L. & Mele, E. J. *Phys. Rev. Lett.* **110**, 046404 (2013).
 - ⁷ Ohtsubo, Y., Le Fèvre, P., Bertran, F. m. c. & Taleb-Ibrahimi, A. *Phys. Rev. Lett.* **111**, 216401 (2013).
 - ⁸ Barfuss, A. *et al. Phys. Rev. Lett.* **111**, 157205 (2013).
 - ⁹ Wang, J. W., Liu, X. H., Mao, S. X. & Huang, J. Y. *Nano Lett.* **12**, 5897–5902 (2012).
 - ¹⁰ Yu, Y., Gu, L., Zhu, C., van Aken, P. A. & Maier, J. *JACS* **131**, 15984–15985 (2009).
 - ¹¹ Qin, J. *et al. ACS Nano* **8**, 1728–1738 (2014).
 - ¹² Zou, Y. & Wang, Y. *ACS Nano* **5**, 8108–8114 (2011).
 - ¹³ Zhou, X., Bao, J., Dai, Z. & Guo, Y.-G. *J. Phys. Chem. C* **117**, 25367–25373 (2013).
 - ¹⁴ Xu, Y. *et al. Phys. Rev. Lett.* **111**, 136804 (2013).
 - ¹⁵ Zhu, H. *et al. Nano Lett.* **13**, 3093–3100 (2013).
 - ¹⁶ Slater, M. D., Kim, D., Lee, E. & Johnson, C. S. *Adv. Funct. Mater.* **23**, 947–958 (2013).
 - ¹⁷ Wang, B., Luo, B., Li, X. & Zhi, L. *Materials Today* **15**, 544 – 552 (2012).
 - ¹⁸ Anji Reddy, M. & Fichtner, M. *J. Mater. Chem.* **21**, 17059–17062 (2011).
 - ¹⁹ Busch, G. & Kebn, R. vol. 11 of *Solid State Physics*, 1 – 40 (Academic Press, 1960).
 - ²⁰ Kang, S., Mo, Y., Ong, S. P. & Ceder, G. *Nano Lett.* **14**, 1016–1020 (2014).
 - ²¹ Wulff, G. *Z. Kristallogr.* **34**, 449530 (1901).
 - ²² Pavone, P., Baroni, S. & de Gironcoli, S. *Phys. Rev. B* **57**, 10421–10423 (1998).
 - ²³ Ashcroft, N. W. & Mermin, N. D. *Solid State Physics* (Brooks/Cole, 2007), third indian reprint edn.
 - ²⁴ Kresse, G. & Furthmüller, J. *Phys. Rev. B* **54**, 11169–11186 (1996).
 - ²⁵ Kresse, G. & Furthmüller, J. *Comput. Mater. Sci.* **6**, 15 – 50 (1996).
 - ²⁶ Perdew, J. P., Burke, K. & Ernzerhof, M. *Phys. Rev. Lett.* **77**, 3865–3868 (1996).
 - ²⁷ Christensen, N. E. & Methfessel, M. *Phys. Rev. B* **48**, 5797–5807 (1993).
 - ²⁸ Blöchl, P. E. *Phys. Rev. B* **50**, 17953–17979 (1994).
 - ²⁹ Hafner, J. *J. Comput. Chem.* **29**, 20442078 (2008).
 - ³⁰ Sabet, S. & Kaghazchi, P. *J. Chem. Phys.* **140**, 191102 (2014).
 - ³¹ Farrow, R. *et al. J. Cryst. Growth* **54**, 507 – 518 (1981).
 - ³² Jette, E. R. & Foote, F. *J. Chem. Phys.* **3**, 605–616 (1935).
 - ³³ Harrison, W. *Electronic Structure and the Properties of Solids* (Dover, New York, 1989).
 - ³⁴ Badt, D., Wengelnik, H. & Neddermeyer, H. *J. Vac. Sc. & Tech. B* **12**, 2015–2017 (1994).
 - ³⁵ Ramstad, A., Brocks, G. & Kelly, P. J. *Phys. Rev. B* **51**, 14504–14523 (1995).
 - ³⁶ Sakama, H., Kawazu, A. & Ueda, K. *Phys. Rev. B* **34**, 1367–1370 (1986).
 - ³⁷ Mittendorfer, F., Seriani, N., Dubay, O. & Kresse, G. *Phys. Rev. B* **76**, 233413 (2007).
 - ³⁸ Soon, A., Wong, L., Delley, B. & Stampfl, C. *Phys. Rev. B* **77**, 125423 (2008).
 - ³⁹ Kaghazchi, P. *RSC Adv.* **4**, 1646–1649 (2014).
 - ⁴⁰ Kaghazchi, P. & Jacob, T. *Phys. Rev. B* **86**, 085434 (2012).
 - ⁴¹ Zhu, T. *et al. Phys. Chem. Chem. Phys.* **15**, 2268–2272 (2013).
 - ⁴² M. Broussely, Ph. Biensan, F. Bonhomme, Ph. Blanchard, S. Herreyre, K. Nechev, and R.J. Staniewicz, *Journal of Power Sources*, **146**, 90 – 96 (2005).
 - ⁴³ J. Vetter, P. Novák, M.R. Wagner, C. Veit, K.-C. Müller, J.O. Besenhard, M. Winter, M. Wohlfahrt-Mehrens, C. Vogler, and A. Hammouche” *Journal of Power Sources* **147**, 269 –281 (2005).